PHILOSOPHICAL MAGAZINE
2018, VOL. 98, NO. 34, 3072–3085
https://doi.org/10.1080/14786435.2018.1516899

Dislocation bending in GaN/step-graded (Al,Ga)N/AlN buffer layers on Si(111) investigated by STM and STEM

Lei Zhang[a,b], Verena Portz[a,c], Michael Schnedler[a], Lei Jin[d], Yuhan Wang[a], Xiaopeng Hao[b], Holger Eisele[e], Rafal E Dunin-Borkowski[a,d] and Philipp Ebert [a]

[a]Peter Grünberg Institut, Forschungszentrum Jülich GmbH, Jülich, Germany; [b]State Key Laboratory of Crystal Materials, Shandong University, Jinan, People's Republic of China; [c]Department of Physics, National Taiwan University, Taipei, Taiwan; [d]Ernst Ruska-Centrum, Forschungszentrum Jülich GmbH, Jülich, Germany; [e]Institut für Festkörperphysik, Technische Universität Berlin, Berlin, Germany

ABSTRACT

The distribution and bending of dislocations in GaN/step-graded (Al,Ga)N/AlN buffer layers grown on Si(111) are investigated by cross-sectional scanning tunnelling microscopy (STM) and scanning transmission electron microscopy (STEM). We observe dislocations with $(a/3)\langle 11\bar{2}0\rangle$-type Burgers vector intersecting the *m*-plane cleavage surface and having line directions bent off the [0001] growth direction toward non-polar directions. The spatial distribution of dislocations intersecting the *m*-plane cleavage surface indicates consecutive bending of dislocations due to strain at interfaces between subsequent lattice mismatched buffer layers and at doping junctions, reducing the density of threading dislocations at the (0001) growth front. No interface misfit dislocations, v-shaped defects, or loss of crystalline quality are observed, demonstrating the high performance of the step-graded (Al, Ga)N/AlN buffer layers on Si for relaxing the lattice constant without creating large defect concentrations.

ARTICLE HISTORY
Received 15 February 2018
Accepted 3 August 2018

KEYWORDS
Dislocation bending; step-graded (Al; Ga)N/AlN; cross-section scanning tunnelling microscopy; nitrides on silicon

1. Introduction

Group III-nitride semiconductors became the material system of choice for next generation optoelectronics and high-power semiconductor devices [1–3]. However, besides GaN and very small AlN (pseudo)substrates, the growth of ternary III-nitride layers suffers from the lack of suitable lattice-matched substrates. Moreover, GaN and AlN substrates are extraordinarily expensive and Si as an inexpensive substrate with large size and good thermal conductivity would be preferable, also in view of combining nitride based optoelectronics with the Si technology [4,5]. Unfortunately, GaN cannot be grown directly on Si, due to back etching effects leading to polycrystalline GaN layers [6–8]. Furthermore, the large lattice and thermal mismatch results in high dislocation

CONTACT Philipp Ebert p.ebert@fz-juelich.de Peter Grünberg Institut, Forschungszentrum Jülich GmbH, 52425 Jülich, Germany

© 2018 Informa UK Limited, trading as Taylor & Francis Group

densities, strain, and cracking, inhibiting successful device fabrication [9]. In order to circumvent these problems, AlN/(Al,Ga)N buffer layers on Si substrates have emerged, allowing a successful strain management as well as reducing the threading dislocation density by bending, annihilation, and immobilisation of dislocations [10–12]. Thus far the spatial evolution and properties of dislocations associated with AlN/(Al,Ga)N buffer layers has been investigated microscopically by transmission electron microscopy (TEM) only [13–18]. However, cross-sectional scanning tunnelling microscopy (STM) and spectroscopy (STS) provides a complimentary insight by probing the type, line direction, charge, and spatial distribution of bent dislocations on $(10\bar{1}0)$ m-plane GaN cross-sectional cleavage surfaces [19–21]. Since the cross-sectional geometry provides access to bent dislocations only, these can be separated from threading dislocations which do not intersect the cleavage plane. Hence, cross-sectional STM provides an insight in the dislocation bending during growth of AlN/(Al,Ga)N buffer layers. These advantages enable us to better understand the dislocation structure of AlN/(Al,Ga)N buffer layers ultimately improving the crystal quality of group III-nitride epitaxial layers on Si and hence the device performance.

Therefore, we investigate the dislocation distribution and bending in GaN/(Al,Ga)N/AlN buffer layers grown on Si using cross-sectional STM. We identify a progressive bending of dislocations with $(a/3)\langle 11\bar{2}0\rangle$-type Burgers vectors due to strain at the interfaces between consecutive lattice mismatched layers, giving rise to peaks in the spatial distribution of bent dislocations intersecting the m-plane cleavage surface. The lack of interface misfit dislocations, v-shaped defects, or loss of crystalline quality confirm the high potential of (Al,Ga)N/AlN buffer layers for relaxing the lattice constant toward that of GaN while reducing the density of threading dislocations on the (0001) growth front.

2. Experiment

For our STM and STS investigations, we cleaved GaN/step-graded (Al,Ga)N/AlN buffer layers grown on Si (111) substrates in ultrahigh vacuum ($p \approx 1 \times 10^{-8}$ Pa) to expose a clean cross-sectional $(10\bar{1}0)$ m-plane surface. The GaN/step-graded (Al,Ga)N/AlN buffer layers were grown by metal organic chemical vapour phase deposition. For improving cleavage, samples cut from full wafers were thinned down mechanically with sandpaper from the Si substrate side to ~ 100 µm and contacted by sputtered Au layers. Directly after cleavage, the fresh cleavage surfaces were investigated by cross-sectional STM and STS without interruption of the vacuum. For the STM and STS measurement, we used electrochemically etched tungsten tips. Note, no dislocations are created in the nitride semiconductor layers during thinning and cleavage in accordance with previous experiments on GaAs [22,23].

The detailed layer sequence, compositions, and thicknesses of the buffer structure have been characterised by energy dispersive x-ray (EDX)

spectroscopy in scanning transmission electron microscopy (STEM) [24]. In addition, a complementary transmission electron microscopy characterisation [25] of the dislocations present in the buffer layers was performed for comparison with the STM measurements. For (S)TEM measurements a thin lamella was cut in cross-sectional m-plane geometry by focussed ion beam.

3. Results

3.1. Transmission electron microscopy

In order to obtain a first overview of the GaN/step-graded (Al,Ga)N/AlN buffer system we performed an EDX elemental mapping by STEM. For identifying and separating the different chemical species, which contributed to the measured EDX spectra, we applied spectral unmixing (SU). We chose a non-negative matrix factorisation (NMF) algorithm for SU, since the resulting non-negative components are correlated with the different chemical species or compounds [26]. Figure 1 illustrates the spatial distribution of the different materials extracted with this decomposition technique. The first three components with largest eigenvalues can be identified on basis of the decomposed EDX spectra shown as insets in the respective two-dimensional maps. They can be attributed to GaN, AlN, and Si, respectively. No further component has eigenvalues exceeding noise. One can clearly recognise five different layers from pure Si to the left, through pure AlN, two layers with different AlN/GaN mixtures and pure GaN to the right. From these data, we extract compositions of the two (Al,Ga)N layers which are in good agreement with the nominally grown ones of $Al_{0.35}Ga_{0.65}N$ and $Al_{0.17}Ga_{0.83}N$. In addition, we obtain layer thicknesses of 300, 320 and 370 nm for the AlN, $Al_{0.35}Ga_{0.65}N$, and $Al_{0.17}Ga_{0.83}N$ buffer layers. In the following, these thicknesses will be used to mark the layer positions in TEM and STM images. Note, the different Si doping within the pure GaN cannot be distinguished with this method. In fact, the GaN consist of 400 nm undoped GaN followed by Si-doped GaN.

Figure 1 also indicates that the interfaces are mostly smooth. Only the interface between the $Al_{0.35}Ga_{0.65}N$ and $Al_{0.17}Ga_{0.83}N$ buffer layers was found in TEM images to exhibit a considerable roughness reaching 50 nm (see dashed lines in Figure 1 (a)). The total (Al,Ga)N buffer layer thickness (320+370 nm) remains, however, constant, as the interface to GaN is smooth again.

Furthermore, we investigated the dislocation structure in the GaN/step-graded (Al,Ga)N/AlN buffer system by using bright-field (BF) and weak-beam dark-field (WDBF) imaging technique under a $\vec{g} - 3\vec{g}$ (with $\vec{g}$ being a reciprocal lattice vector) [27]. Figure 2 shows WBDF and BF images (left and right, respectively) for $\vec{g} = 0002$ (top) and $\vec{g} = 11\bar{2}0$ (bottom). According to the $\vec{g} \cdot \vec{b} = 0$ criterion, with $\vec{b}$ being the Burgers vector, the upper and lower

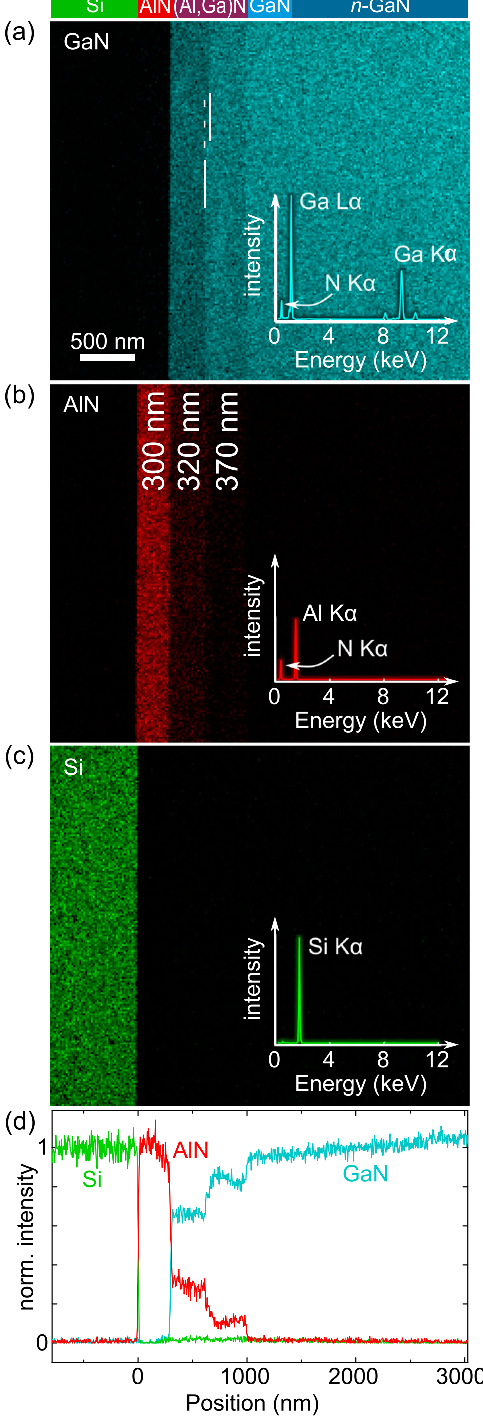

Figure 1. Cross-sectional energy dispersive x-ray spectroscopy by scanning transmission electron microscopy of the GaN/step-graded (Al,Ga)N/AlN buffer system grown on Si. (a), (b), and (c) show the spatial distribution and the corresponding decomposed EDX spectra of GaN, AlN and Si, respectively, extracted using a non-negative matrix factorisation algorithm for spectral decomposition. (d) Composition profiles along the *c* growth direction.

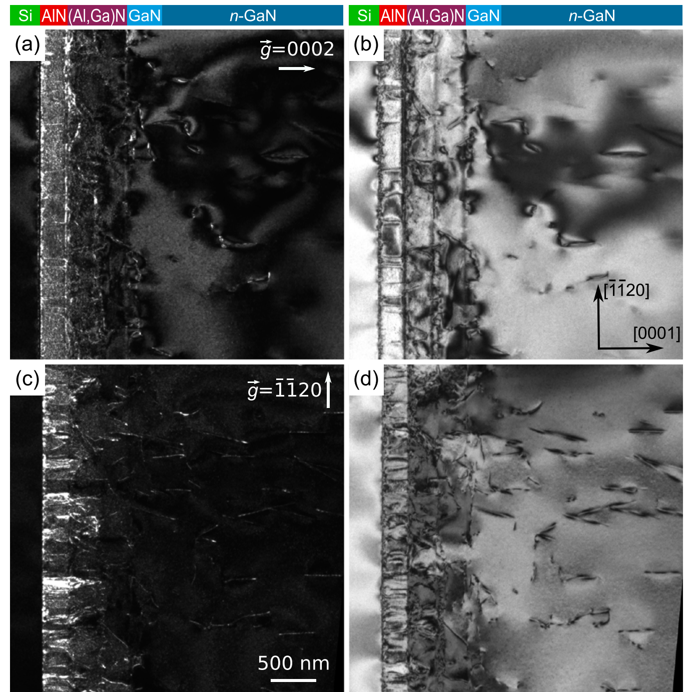

Figure 2. Weak-beam dark-field (a,c) and bright-field (b,d) images of the dislocation structure in the GaN/step-graded (Al,Ga)N/AlN buffer system grown on Si. (a,b) show dislocations with *c*-type and (c,d) with *a*-type Burgers vectors.

frames show the dislocation lines of dislocations with c-type (ie $\vec{b}_c = c[0001]$) and a-type (ie $\vec{b}_a = (a/3)[11\bar{2}0]$) Burgers vector, respectively. The TEM images also reveal that the dominating dislocations are those with a-type Burgers vector. They initially start in the AlN layer parallel to the [0001] growth direction (horizontal direction in the TEM image) as pure edge dislocations. Close to every interface a bending of dislocations toward non-polar directions is observed, in addition to dislocations which keep their [0001] line direction. However, no interface misfit dislocation network is found. Note, the layer markings on top illustrate only the approximate interface positions. For a more detailed understanding, the bending of dislocation is investigated in the following by scanning tunnelling microscopy on cross-sectionally cleaved m-plane surfaces. This geometry is particularly attractive, since only bent dislocations intersect the cleaved m-plane surfaces. All other dislocations remain in subsurface layers and do not interfere with the analysis of bent dislocations.

3.2. Scanning tunnelling microscopy and spectroscopy

Figure 3 shows a composition of cross-sectional STM overview images of the GaN/step-graded (Al,Ga)N/AlN buffer system grown on Si. The surface

morphology visible in Figure 3(a) is governed by atomically flat terraces, separated by steps. The Si substrate (not shown here) was identified by its typical 2×1 dimer row reconstructed Si(111) terraces. At first view, there is very little hint which layers are visible within the group III-nitride buffer system, except in the upper left corner, where an interface line can be discerned with pronounced instabilities on the left side of the interface. For the identification of the different nitride layers, we acquired so-called current imaging tunnelling spectroscopy maps from a raster of tunnelling spectra. These show a significantly lower, almost vanishing tunnel current at positive voltages within the AlN layer (see current profile in Figure 3 (c)), due to the larger band gap and different energy position of the surface states [28,29]. The lack of tunnel current at positive voltages in the AlN layer leads to instabilities in the constant-current image. Hence, this allows the identification of the AlN layer in the upper left corner. The

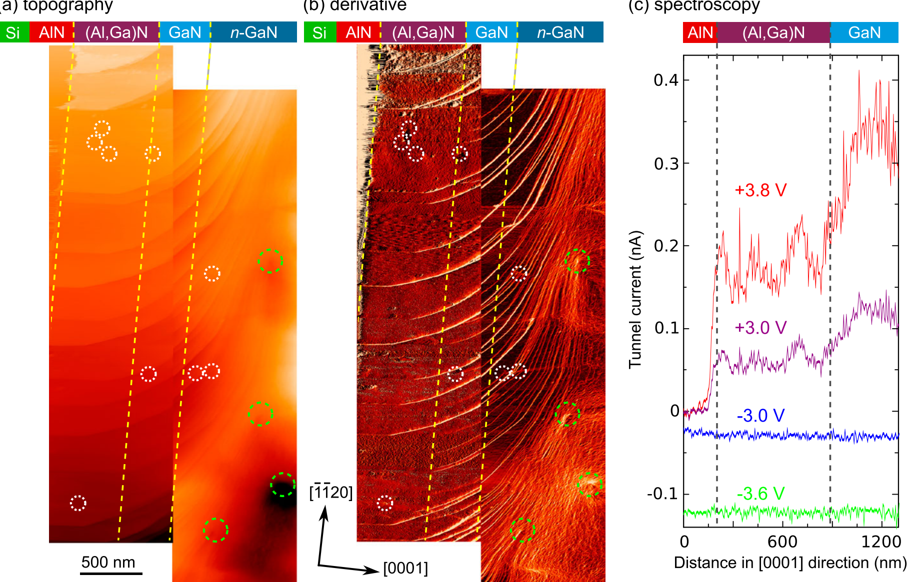

Figure 3. Scanning tunnelling microscopy overview of the GaN/step-graded (Al,Ga)N/AlN buffer system grown on Si. (a) Mosaic of constant-current STM images acquired at a tunnelling voltage of +4.5 V and a current of 70 pA. (b) Derivative STM image showing the amplitude of the gradient to highlight the steps on the cleavage surface. Some monoatomic high steps terminate at intersection points of dislocations. The dislocations exhibit a Burgers vector of the type $(a/3)\langle 11\bar{2}0\rangle$ and their intersection points, identified in highly magnified STM images, are marked by white dotted circles (for a higher magnification of dislocations intersection points see Figure 4). In addition, we observed step bunching areas marked by larger green dotted circles. They do not contain any terminating step. We attribute these to dislocations with $\pm c[0001]$ Burgers vectors intersecting the cleavage surface. (c) Identification of the different group III-nitride semiconductor layers using current profiles in [0001] growth direction at different voltages extracted from a grid of tunnelling spectra. At negative voltages, no differences appear between the layers. In contrast, the current profiles at positive voltages show no current within the AlN layer, but a clear current in the following (Al,Ga)N and GaN layers.

contrast between the other layers is much weaker and hardly discernable. However, using the growth sequence, the previously discussed EDX-STEM analysis, and the identification by tunnelling spectroscopy of the AlN/(Al, Ga)N interface as a reference, the approximate positions of all interfaces can be indicated on this basis.

The most pronounced characteristic of the morphology of the cross-sectional cleavage surface of the buffer layers are steps separating atomically flat terraces. In order to highlight the steps, Figure 3(b) presents the derivative images (magnitude of gradient, $|\nabla z(x,y)|$) of the constant-current STM images. Steps appear as brighter lines. A rather low density of multi monolayer (ML) high steps start at the AlN/Si interface (not visible in Figure 3) and are oriented along the [0001] direction. These high [0001] oriented steps cross the heterointerface between AlN and the $Al_{0.35}Ga_{0.65}N$ layer without changing direction. Further on, the high steps slowly bend in the following layers and fan out exposing individual one ML high steps. This leads to a significant increase of the step density in the GaN layer. The large step concentration further to the right suggests an increasingly compressively strained *n*-doped GaN layer [28,30]. This can be attributed to further (Ga,In)N layers with large lattice mismatch grown on top of the buffer system (outside of the scanning range of Figure 3).

A further interesting aspect is that the atomically flat terraces of the (Al,Ga)N and AlN layers exhibit exactly the same orientation, ie same normal vector orientation (neglecting the initial nucleation layer). Hence, no inclination of the $(10\bar{1}0)$ cleavage plane between different layers can be detected in the STM images. This indicates that no misorientation, grain boundaries, or v-shaped defects are present in the (Al,Ga)N/AlN buffer layers. Hence, the (Al,Ga)N/AlN buffer layer possesses high crystalline quality.

At this stage, we address the presence of dislocations in the buffer layers. Dislocations intersecting the cleavage plane give rise to suddenly terminating single monolayer high steps [19,31]. In Figure 3 these dislocation intersection points are marked by white dotted circles. Since in the overview image details of dislocations are hard to see, Figure 4(a) shows a topographic constant-current STM image of a nearby area at higher magnification. Again dislocations intersect the cleavage plane at the locations marked by black and white dotted circles. At a closer look, the contrasts around the intersection points of dislocations in Figure 4(a) indicate that each dislocation distorts the surface and induces a displacement field. The derivative of the STM image shown in Figure 4(b) can be used to highlight and analyse the displacement fields of the dislocations [19–21]. Starting at two termination points of steps, particularly extended and highly directional displacement fields can be recognised (see blue arrows), which shows up in the derivative image in Figure 4 (b), too. The extended directional displacement fields arise from shallow subsurface dislocation cores, whose displacement fields relax toward the surface [19]. The extend and orientation

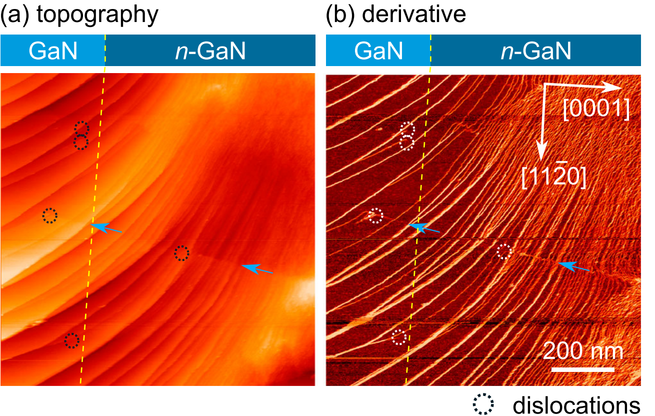

Figure 4. Zoom of a cross-sectional surface area in the vicinity of the undoped GaN/*n*-type GaN interface measured by scanning tunnelling microscopy. (a) Topographic constant-current STM image and (b) derivative image showing the amplitude of the gradient for highlighting the steps and the displacement fields near dislocations on the cross-sectional (10$\bar{1}$0) cleavage surface. In this area, five dislocations are found to intersect the cleavage surface (steps terminating suddenly). The strain fields introduced by the dislocations induce distortions of the surface plane. In some cases, these distortions extend far away from the intersection point (arrows), indicating the presence of shallow subsurface dislocation cores over extended distances.

show that the dislocation line is running quite parallel to the surface with an inclination toward the ⟨11$\bar{2}$0⟩ direction of 10–15° [21].

Furthermore, we extracted the local density of dislocations intersecting the (10$\bar{1}$0) cleavage surface as a function of the distance to the Si substrate, ie with progressing growth (Figure 5). For this, we identified the intersection points of a total of 50 dislocations observed in various STM images and extracted the distance to the AlN/Si interface. The spatial distribution of the dislocation intersection points reveals several interesting characteristics of the GaN/step-

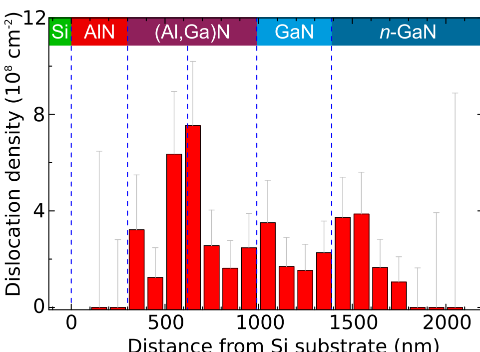

Figure 5. Spatial distribution of intersection points of bent dislocations at the (10$\bar{1}$0) cleavage surfaces of the GaN/step-graded (Al,Ga)N/AlN buffer system grown on Si(111) as a function of the distance of the intersection points of dislocations from the AlN/Si interface as measured in STM images.

graded (Al,Ga)N/AlN buffer system: (i) We observed no dislocation in the AlN layer beyond the initial nucleation layer. (ii) A dislocation density between 1×10^8 and $\sim 8 \times 10^8$ cm^{-2} is found in the (Al,Ga)N, undoped GaN, and the first 500 to 600 nm of n-doped GaN layer. (iii) We observed no specific localisation of dislocations directly at the heterointerfaces. However, directly after every interface the dislocation density peaks (Figure 5). Note, the high dislocation density just before the $Al_{0.17}Ga_{0.83}N/Al_{0.35}Ga_{0.65}N$ interface is likely resulting from the large interface roughness observed only for this interface in TEM images. This roughness effect is not present for the other smooth interfaces, and hence the dislocation density clearly peaks after the interface in the growth direction.

4. Discussion

Group III-nitride semiconductors in the wurtzite structure typically contain three types of dislocations, which are classified according to their Burgers vector $\vec{b}$ and assuming a line direction in [0001]: (i) a pure edge dislocation with $\vec{b}_a = (a/3)\langle 11\bar{2}0\rangle$, (ii) a pure screw dislocation with $\vec{b}_c = c\langle 0001\rangle$, and (iii) a mixed-type dislocation with $\vec{b}_{c+a} = \vec{b}_a + \vec{b}_c$ [32]. In the TEM images, the dominating type of dislocations has an a-type Burgers vector. c-type Burgers vectors occur with a significantly lower concentration. We also observed a few a and c-type mixed-type Burgers vectors. On this basis, we turn to the dislocations detected in the STM images.

All dislocations observed in the STM images induce a one monolayer high step on the $(10\bar{1}0)$ surface, corresponding to a Burgers vector of the type $\pm < (a/3)[11\bar{2}0]$ or $\pm(a/3)[\bar{2}110]$, each tilted by 30° with respect to the surface normal [19]. In principle, the formation of a 1 ML high step would also be compatible with mixed-type dislocations, but their concentration is significantly lower [33–35] due to the higher energy related to the longer Burgers vector [36]. Dislocations with Burgers vectors along the c direction, ie lying fully within the surface plane, cannot be observed in large-scale images without lateral atomic resolution. Hence, all dislocations, which we observed in STM images have Burgers vectors of the type $(a/3)\langle 11\bar{2}0\rangle$. Note, even if a dislocation with c-type Burgers vector intersects the cleavage surface, we cannot detect it in STM images without lateral atomic resolution [19].

Dislocations with Burgers vectors of the type $(a/3)\langle 11\bar{2}0\rangle$ are initially formed at the AlN/Si interface (or other heterointerfaces) as pure edge dislocations with [0001] line direction. If these dislocations remain unchanged during progressing growth, ie no bending of the dislocation line occurs, they would never intersect the m-plane cleavage surface. Hence, observing dislocations intersecting the cleavage surface demonstrates that a bending of the dislocation line away

from the [0001] direction toward non-polar directions occurred. The shallow subsurface dislocation lines observed in Figure 4 indicate that a bending of minimum 10 to 15° incurred. Other dislocations have very localised displacement fields and are thus intersecting the cleavage surface almost perpendicularly, ie are bent by almost 90°. Note, the bent dislocations lose the pure edge character and become mixed screw and edge dislocations.

The spatial distribution of the dislocation intersections with the cleavage surface in Figure 5 provides some insight where the dislocation bending occurs. First, no dislocations can be observed within the AlN layer, indicating that no bending occurs in this layer. This agrees also well with the [0001] line direction observed in the TEM images in Figure 2. Second, the density of bent dislocation is found to peak shortly after every following interface. For example, dislocations start to intersect the *m*-plane cleavage surface in the first part of the $Al_{0.35}Ga_{0.65}N$ buffer. This points to a start of the dislocation bending at the $Al_{0.35}Ga_{0.65}N$/AlN interface. Note, the STM and TEM images point to the absence of misfit dislocations at all interfaces studied here, in contrast to InN/GaN interfaces, where the start of many single ML high steps reveal the presence of an interface misfit dislocation network [37]. Considering the absence of interface misfit dislocations, the bending of the threading edge dislocations can be related to the strain field in the interface region: Due to the lattice mismatch at the $Al_{0.35}Ga_{0.65}N$/AlN interface, the stress changes from tensile to compressive at the interface. Since dislocations have a tensile and a compressive side due to the insertion of a half plane, the tensile side of the dislocation will be attracted by the compressive $Al_{0.35}Ga_{0.65}N$ side of the interface. This interaction will gradually increase the inclination angles of threading dislocations with respect to the [0001] growth direction balanced by the additional line length, hence inducing dislocation bending during progressing growth [16, 38–40].

Analogous effects can be expected to occur at the $Al_{0.17}Ga_{0.83}N/Al_{0.35}Ga_{0.65}N$ and GaN/$Al_{0.17}Ga_{0.83}N$ interfaces, since no interface misfit dislocations were found at these interfaces either. Indeed, the density of dislocations intersecting the *m*-plane cleavage surface peaks slightly after these interfaces, suggesting an additional bending of dislocation lines at these interfaces.

Furthermore, the density of bent dislocations also peaks after the undoped to Si-doped GaN interface in Figure 5. This can be related to the fact that the interface between undoped and Si-doped GaN(0001) is also strained, although somewhat less than the previous interfaces [41]. GaN(0001) layers with different Si doping concentrations exhibit slightly different lattice constants, giving rise to compressive strain in *a* direction on the Si-doped GaN side of the interface [42,43]. This is supported by *in-situ* curvature measurements showing an increase of compressive strain upon Si doping at growth temperature [44], where dislocations form and propagate during progressive growth. Hence, dislocations can again interact with the strain field at the interface between undoped and Si-doped GaN, leading to a bending of the dislocation lines and

thus to the peak of the dislocation density after the interface in the lower part of the *n*-doped GaN layer. This demonstrates that modulation doped group III-N layers contribute to the reduction of the threading dislocation density by dislocation line bending, too.

Finally, the STM images show bunching of steps in the *n*-doped GaN layer, but without termination of steps. These bunching sites are marked by green dashed circles on the right side of Figure 3 (b). They occur in concentration of about 1×10^8 cm^{-2}. This can be correlated with intersection points of dislocations with *c*-type Burgers vector on basis of the density of these dislocations in the TEM images and considering that the *c*-type Burgers vector does not induce steps on the *m*-plane cleavage surfaces and thus is only visible with atomic resolution. However, the cleavage steps interact with the strain field of the dislocations, leading to the pronounced step bunching sites, thereby providing a hint of the presence of such dislocations.

5. Conclusions

In summary, our cross-sectional STM and STEM investigation demonstrates successive dislocation bending of initially pure edge dislocations with a $(a/3)\langle 11\bar{2}0\rangle$-type Burgers vector during progressing growth at every heterointerface and doping junction. The bending is initiated by strained heterointerfaces and doping junctions with in-plane tensile to compressive transitions. No misorientation, small angle grain boundaries, or v-shaped defects occur in significant concentrations. Successive dislocation bending leads to a significant reduction of the threading dislocation density on the (0001) growth plane, while the lattice constants are adjusted to that of GaN through the different buffer layers without losing the high crystalline quality.

Disclosure statement

No potential conflict of interest was reported by the authors.

Funding

The authors thank K.-H. Graf for technical support and U. Breuer for SIMS measurements. LZ acknowledges the Office of the China Postdoctoral Council (OCPC) of the Ministry of Human Resources and Social Security (MoHRSS) and the Forschungszentrum Jülich GmbH for a fellowship in the Jülich OCPC Programme for the Involvement of Postdocs in Bilateral Collaboration Projects with China. This work was funded by the Deutsche Forschungsgemeinschaft (DFG, German Research Foundation) [grant number 398305088].

ORCID

Philipp Ebert http://orcid.org/0000-0002-2022-2378

References

[1] Semond F., *Epitaxial challenges of GaN on silicon*, MRS Bull. 40 (2015), pp. 412–417. doi:10.1557/mrs.2015.96.

[2] Jia H., Guo L., Wang W., and Chen H., *Recent progress in GaN-based light-emitting diodes*, Adv. Mater. 21 (2009), pp. 4641–4646. doi:10.1002/adma.200901349.

[3] Amano H., *Progress and prospect of the growth of wide-band-gap group III nitrides: Development of the growth method for single-crystal bulk GaN*, Jpn. J. Appl. Phys. 52 (2013), pp. 050001. Available at http://stacks.iop.org/1347-4065/52/i=5R/a=050001.

[4] Kadir A., Huang C.C., Lee K.E.K., Fitzgerald E.A., and Chua S.J., *Determination of alloy composition and strain in multiple AlGaN buffer layers in GaN/Si system*, Appl. Phys. Lett. 105 (2014), pp. 232113. doi:10.1063/1.4904007.

[5] Shen X.Q., Takahashi T., Matsuhata H., Ide T., and Shimizu M., *Self-generated micro-cracks in an ultra-thin AlN/GaN superlattice interlayer and their influences on the GaN epilayer grown on Si(110) substrates by metal-organic chemical vapor deposition*, Cryst. Eng. Commun. 17 (2015), pp. 5014–5018. doi:10.1039/C5CE00929D.

[6] Dadgar A., Poschenrieder M., Blasing J., Fehse K., Diez A., and Krost A., *Thick, crack-free blue light-emitting diodes on Si(111) using low-temperature AlN interlayers and in situ* Si_xN_y *masking*, Appl. Phys. Lett. 80 (2002), pp. 3670–3672. doi:10.1063/1.1479455.

[7] Zhang B. and Liu Y., *A review of GaN-based optoelectronic devices on Silicon substrate*, Chin. Sci. Bull. 59 (2014), pp. 1251–1275. doi:10.1007/s11434-014-0169-x.

[8] Hsiao F.M., Schnedler M., Portz V., Huang Y.C., Huang B.C., Shih M.C., Chang C.W., Tu L.W., Eisele H., Dunin-Borkowski R.E., Ebert Ph., and Chiu Y.P., *Probing defect states in polycrystalline GaN grown on Si(111) by sub-bandgap laser-excited scanning tunneling spectroscopy*, J. Appl. Phys. 121 (2017), pp. 015701. doi:10.1063/1.4972563.

[9] Feng B., Deng B., Fu Y., Liu L.G., Li Z.C., Feng M.X., Zhao H.M., and Sun Q., *Efficiency improvement of GaN on-silicon thin-film light-emitting diodes with optimized via-like n-electrodes*, Semicond. Sci. Technol. 32 (2016), pp. 075009. Available at http://stacks.iop.org/0268-1242/32/i=7/a=075009.

[10] Xiang R., Fang Y.Y., Dai J., Zhang L., Su C., Wu Z., Yu C., Xiong H., Chen C., and Hao Y., *High quality GaN epilayers grown on Si (111) with thin nonlinearly composition-graded* $Al_xGa_{1-x}N$ *interlayers via metal-organic chemical vapor deposition*, J. Alloys Comp. 509 (2011), pp. 2227–2231. Available at http://www.sciencedirect.com/science/article/pii/S0925838810027234.

[11] Cheng J., Yang X., Ling Sang L.G., Zhang J., Wang J., He C., Zhang L., Wang M., Xu F., Tang N., Qin Z., Wang X., and Shen B., *Growth of high quality and uniformity AlGaN/GaN heterostructures on Si substrates using a single AlGaN layer with low Al composition*, Sci. Rep. 6 (2016), pp. 23020. doi:10.1038/srep23020.

[12] Sun Y., Zhou K., Sun Q., Liu J., Feng M., Li Z., Zhou Y., Zhang L., Li D., Zhang S., Ikeda M., Liu S., and Yang H., *Room-temperature continuous-wave electrically injected InGaN-based laser directly grown on Si*, Nat. Photon. 10 (2016), pp. 595–599. doi:10.1038/nphoton.2016.158.

[13] Gradeçak S., Stadelmann P., Wagner V., and Ilegems M., *Bending of dislocations in GaN during epitaxial lateral overgrowth*, Appl. Phys. Lett. 85 (2004), pp. 4648–4650. doi:10.1063/1.1823593.

[14] Leung B., Han J., and Sun Q., *Strain relaxation and dislocation reduction in AlGaN step-graded buffer for crack-free GaN on Si (111)*, Phys. Stat. Sol. (c) 11 (2014), pp. 437–441. doi:10.1002/pssc.201300690.

[15] Raghavan S., Weng X., Dickey E., and Redwing J.M., *Correlation of growth stress and structural evolution during metalorganic chemical vapor deposition of GaN on (111) Si*, Appl. Phys. Lett. 88 (2006), pp. 041904. doi:10.1063/1.2168020.

[16] Yang Y., Xiang P., Liu M., Chen W., He Z., Han X., Ni Y., Yang F., Yao Y., Wu Z., Liu Y., and Zhang B., *Effect of compositionally graded AlGaN buffer layer grown by different functions of trimethylaluminum flow rates on the properties of GaN on Si (111) substrates*, J. Cryst. Growth 376 (2013), pp. 23–27. Available at http://www.sciencedirect.com/science/article/pii/S0022024813002923.

[17] Brunner F., Mogilatenko A., Kueller V., Knauer A., and Weyers M., *Stress evolution during $Al_xGa_{1-x}N$/ AlN growth on sapphire*, J. Cryst. Growth 376 (2013), pp. 54–58. Available at http://www.sciencedirect.com/science/article/pii/S0022024813002728.

[18] Massabuau F.C.P., Rhode S.L., Horton M.K., O'Hanlon T.J., Kovács A., Zielinski M.S., Kappers M.J., Dunin-Borkowski R.E., Humphreys C.J., and Oliver R.A., *Dislocations in AlGaN: Core structure, atom segregation, and optical properties*, Nano Lett. 17 (2017), pp. 4846–4852. doi:10.1021/acs.nanolett.7b01697.

[19] Ebert Ph., Ivanova L., Borisova S., Eisele H., Laubsch A., and Dähne M., *Electronic properties of dislocations in GaN investigated by scanning tunneling microscopy*, Appl. Phys. Lett. 94 (2009), pp. 062104. doi:10.1063/1.3073741.

[20] Weidlich P.H., Schnedler M., Eisele H., Dunin-Borkowski R., Ebert Ph., *Repulsive interactions between dislocations and overgrown v-shaped defects in epitaxial GaN layers*, Appl. Phys. Lett. 103 (2013), pp. 142105. Available at http://scitation.aip.org/content/aip/journal/apl/103/14/10.1063/1.4823474.

[21] Weidlich P.H., Schnedler M., Portz V., Eisele H., Strauß U., Dunin-Borkowski R.E., Ebert Ph., *Tracking the subsurface path of dislocations in GaN using scanning tunneling microscopy*, J. Appl. Phys. 118 (2015), pp. 035302. Available at http://scitation.aip.org/content/aip/journal/jap/118/3/10.1063/1.4926789.

[22] Cox G., Ebert Ph., Poppe U., Simon M., and Urban K., *Dislocation reaction on p-doped GaAs(011) observed by scanning tunneling microscopy*, Ultramicroscopy 42-44 (1992), pp. 776–780. Available at http://www.sciencedirect.com/science/article/pii/030439919290357P.

[23] Ebert Ph., Domke C., and Urban K., *Direct observation of electrical charges at dislocations in GaAs by cross-sectional scanning tunneling microscopy*, Appl. Phys. Lett. 78 (2001), pp. 480–482. doi:10.1063/1.1341219.

[24] Ernst Ruska-Centre for Microscopy and Spectroscopy with Electrons (ER-C). *FEI Titan G2 80-200 Crewley*, J. Large-scale Res. Facil. 2 (2016), pp. A43. doi:10.17815/jlsrf-2-68.

[25] Ernst Ruska-Centre for Microscopy and Spectroscopy with Electrons (ER-C). *FEI Tecnai G2 F20*, J. Large-scale Res. Facil. 2 (2016), pp. A77. doi:10.17815/jlsrf-2-138.

[26] de la Peña F., Ostasevicius T., Fauske V.T., Burdet P., Jokubauskas P., Nord M., Prestat E., Sarahan M., MacArthur K.E., Johnstone D.N., Taillon J., Caron J., Furnival T., Eljarrat A., Mazzucco S., Migunov V., Aarholt T., Walls M., Winkler F., Martineau B., Donval G., Hoglund E.R., Alxneit I., Hjorth I., Zagonel L.F., Garmannslund A., Gohlke C., Iyengar I., and Chang H.W., *Hyperspy software package*, doi:10.5281/zenodo.583693 (2011).

[27] Cockayne D.J.H., Ray I.L.F., and Whelan M.J., *Investigations of dislocation strain fields using weak beams*, Philos. Mag. 20 (1969), pp. 1265–1270. doi:10.1080/14786436908228210.

[28] Portz V., Schnedler M., Duchamp M., Hsiao F.M., Eisele H., Carlin J.F., Butté R., Grandjean N., Dunin-Borkowski R.E., and Ebert Ph., *Strain and compositional fluctuations in $Al_{0.81}In_{0.19}N$/GaN heterostructures*, Appl. Phys. Lett. 109 (2016), pp. 132102. doi:10.1063/1.4963184.

[29] Schnedler M., Portz V., Eisele H., Dunin-Borkowski R.E., and Ebert Ph., *Polarity-dependent pinning of a surface state*, Phys. Rev. B 91 (2015), pp. 205309. doi:10.1103/PhysRevB.91.205309.

[30] Quadbeck P., Ebert Ph., Urban K., Gebauer J., and Krause-Rehberg R., *Effect of dopant atoms on the roughness of III-V semiconductor cleavage surfaces*, Appl. Phys. Lett. 76 (2000), pp. 300. doi:10.1063/1.125726.

[31] Cox G., Szynka D., Poppe U., Graf K.H., Urban K., Kisielowski-Kemmerich C., Krüger J., and Alexander H., *Scanning tunneling microscopy of crystal dislocations in gallium arsenide*, Phys. Rev. Lett. 64 (1990), pp. 2402–2405. doi:10.1103/PhysRevLett.64.2402.

[32] Narayanan V., Lorenz K., Kim W., and Mahajan S., *Gallium nitride epitaxy on (0001) sapphire*, Philos. Mag. A 82 (2002), pp. 885–912. doi:10.1080/01418610208240008.

[33] Wu X.H., Brown L.M., Kapolnek D., Keller S., Keller B., DenBaars S.P., and Speck J.S., *Defect structure of metal-organic chemical vapor deposition-grown epitaxial (0001) GaN/Al_2O_3*, J. Appl. Phys. 80 (1996), pp. 3228–3237. doi:10.1063/1.363264.

[34] Grandjean N., Massies J., Vennégués P., Leroux M., Demangeot F., Renucci M., and Frandon J., *Molecular-beam epitaxy of gallium nitride on (0001) sapphire substrates using ammonia*, J. Appl. Phys. 83 (1998), pp. 1379–1383. doi:10.1063/1.366840.

[35] Xin Y., Pennycook S.J., Browning N.D., Nellist P.D., Sivananthan S., Omnes F., Beaumont B., Faurie J.P., and Gibart P., *Direct observation of the core structures of threading dislocations in GaN*, Appl. Phys. Lett. 72 (1998), pp. 2680–2682. doi:10.1063/1.121097.

[36] D. Hull, D.J. Bacon, *Introduction to dislocations*. 5th ed. Elsevier, Amsterdam, 2011. https://doi.org/10.1016/C2009-0-64358-0

[37] Eisele H., Schuppang J., Schnedler M., Duchamp M., Nenstiel C., Portz V., Kure T., Bügler M., Lenz A., Dähne M., Hoffmann A., Gwo S., Choi S., Speck J.S., Dunin-Borkowski R.E., and Ebert Ph., *Intrinsic electronic properties of high-quality wurtzite InN*, Phys. Rev. B 94 (2016), pp. 245201. doi:10.1103/PhysREvB.94.245201.

[38] Romanov A.E. and Speck J.S., *Stress relaxation in mismatched layers due to threading dislocation inclination*, Appl. Phys. Lett. 83 (2003), pp. 2569–2571. doi:10.1063/1.1613360.

[39] Follstaedt D.M., Lee S.R., Allerman A.A., and Floro J.A., *Strain relaxation in AlGaN multilayer structures by inclined dislocations*, J. Appl. Phys. 105 (2009), pp. 083507. doi:10.1063/1.3087515.

[40] Raghavan S., Manning I.C., Weng X., and Redwing J.M., *Dislocation bending and tensile stress generation in GaN and AlGaN films*, J. Cryst. Growth 359 (2012), pp. 35–42. Available at http://www.sciencedirect.com/science/article/pii/S0022024812005726.

[41] Eisele H., Ivanova L., Borisova S., Dähne M., Winkelnkemper M., and Ebert Ph., *Doping modulation in GaN imaged by cross-sectional scanning tunneling microscopy*, Appl. Phys. Lett. 94 (2009), pp. 162110. doi:10.1063/1.3123258.

[42] Polian A., Grimsditch M., and Grzegory I., *Elastic constants of gallium nitride*, J. Appl. Phys. 79 (1996), pp. 3343–3344. Available at http://scitation.aip.org/content/aip/journal/jap/79/6/10.1063/1.361236.

[43] Romano L.T., de Walle C.G.V., Ager III J.W., Götz W., and Kern R.S., *Effect of Si doping on strain, cracking, and microstructure in GaN thin films grown by metalorganic chemical vapor deposition*, J. Appl. Phys. 87 (2000), pp. 7745–7752. doi:10.1063/1.373529.

[44] Dadgar A., Bläsing J., Diez A., and Krost A., *Crack-free, highly conducting GaN layers on Si substrates by Ge doping*, Appl. Phys. Expr. 4 (2011), pp. 011001. doi:10.1143/APEX.4.011001.